Layerwise Analyses of Compact and Thin-Walled Beams Made of Viscoelastic Materials

Matteo Filippi[1]
Department of Mechanical and Aerospace Engineering,
Politecnico di Torino,
Torino 10129, Italy
e-mail: matteo.filippi@polito.it

Erasmo Carrera
Professor of Aerospace Structures and Aeroelasticity
Department of Mechanical and Aerospace Engineering,
Politecnico di Torino,
Torino 10129, Italy
e-mail: erasmo.carrera@polito.it

Andrea M. Regalli
Department of Mechanical and Aerospace Engineering,
Politecnico di Torino,
Torino 10129, Italy
e-mail: andreamariaregalli@yahoo.it

This paper evaluates the vibration characteristics of structures with viscoelastic materials. The mechanical properties of viscoelastic layers have been described with the complex modulus approach. The equations of motion are derived using the principle of virtual displacement (PVD), and they are solved through the finite element method (FEM). Higher-order beam elements have been derived with the Carrera Unified Formulation (CUF), which enables one to go beyond the assumptions of the classical one-dimensional (1D) theories. According to the layerwise approach, Lagrange-like polynomial expansions have been adopted to develop the kinematic assumptions. The complex nonlinear dynamic problem has been solved through an iterative technique in order to consider both constant and frequency-dependent material properties. The results have been reported in terms of frequencies and modal loss factors, and they have been compared with available results in the literature and numerical three-dimensional (3D) finite element (FE) solutions. The proposed beam elements have enabled bending, torsional, shell-like, and coupled mode shapes to be detected. [DOI: 10.1115/1.4034023]

1 Introduction

The viscoelastic structures are widely used in several engineering fields due to their intermediate characteristics between elastic solids and viscous fluids. The most common applications of viscoelastic materials are in the damping technology where the ability to retain retractions and, consequently, dynamic deformations, is exploited. Therefore, they are usually adopted in the noise control of vehicles, airplanes, trains, engines, and turbomachinery [1]. Passive damping treatments mainly consist of thin/moderately thick viscoelastic layers embedded on surfaces (unconstrained layer damping) or constrained between stiffer components (constrained layer damping) [2]. The study of their dynamics essentially involves three main issues: (a) the modeling of material properties; (b) the solution of nonlinear complex eigenvalue problems; and (c) the kinematic modeling of the structure. First, the characterization of viscoelastic materials is performed through dedicated tests such as creep, stress relaxation, and dynamic mechanical analysis, which enable the constitutive relations to be interpolated for limited ranges of frequencies at different temperatures [3,4]. As far as solving techniques are concerned, several methods have been developed for the prediction of complex eigenvalues and corresponding eigenvectors, such as the modal strain energy technique [5,6], the direct frequency response method [7], the iterative complex eigensolution [8], and the asymptotic solution method [9,10]. More details about these methodologies can be found in Ref. [11]. The last aspect, which is the main topic of this paper, concerns the used assumptions for the description of the kinematics of the viscoelastic structures. Since damping treatments are conceived to maximize shear deformations of the viscoelastic layer, an accurate prediction of the stress distribution is of primary importance. For this reason, many displacement theories based on beam, plate/shell and solid assumptions have been proposed using analytical and numerical approaches. For instance, Kerwin [12] analytically solved the vibrational problem for simply supported or infinitely long viscoelastic beams. The lack of generality of Kerwin's theory was overcome by Di Taranto [13], which considered finite-length beams subjected to arbitrary boundary conditions. Over the years, other examples of analytical solutions were proposed by Mead and Markus [14], Yan and Dowell [15], Rao [16] and Bhimaraddi [17]. With the purpose of modeling more complex configurations, the FEM has been extended to the viscoelastic problem. According to the sandwich modeling technique, several beam [10,18–20] and plate [9,21] elements have been proposed in the literature. In these works, Euler–Bernoulli and Kirchoff–Love theories were used for assuming the displacement field of the constraining layers, whereas the soft-core kinematics was approximated by the first-order shear deformation models, namely the Timoshenko and Reissner–Mindlin theories. As stated in Ref. [22], these kinematic assumptions imply that the structure does not experience significant strains or stresses associated with the thickness direction. Hence, this hypothesis may lead to inaccurate results when, for instance, a thick viscoelastic layer is considered. Significant improvements can be achieved using higher-order theories, such as Refs. [7], [22], and [23].

Another usual technique to simulate the behavior of viscoelastic structures is the use of commercial software, which enables us to combine different FEs (beam, plate, and solid FEs). Useful insights about this methodology were provided in Refs. [24] and [25], where MSC.NASTRAN FEs were used to model three-layered planar structures. In particular, plate and solid assemblies, full-3D solutions, and equivalent FEs were evaluated in terms of accuracy and computational costs. Although 3D models provide accurate results, their use may involve two main problems, namely a high computational cost for complex geometries and numerical pathologies such as the shear-locking, which require the use of dedicated numerical techniques (reduced selective integration, MITC, etc.) [25,26].

To provide an alternative to the 3D modeling preserving the numerical efficiency of 1D theories, this paper presents the vibrational study of viscoelastic structures through an advanced beam formulation. The higher-order beam theories have been derived from the CUF [27], which allows to conceive an infinite number of kinematic theories. Within the CUF framework, the componentwise (CW) approach has been here adopted to approximate the displacement field of each structural component. The CW approach exploits the inherent capability of Lagrange-type expansions (LEs) CUF beam models to be assembled at the cross section level. The CW methodology allows only beam elements to be used to model each component of the structures (constraining layer, base, viscoelastic core, etc.) with arbitrary kinematic assumptions, which depend on the characteristics of the components (deformability, mechanical properties, etc.). Moreover, only physical surfaces are employed to build the mathematical model.

[1]Corresponding author.

Contributed by the Technical Committee on Vibration and Sound of ASME for publication in the Journal of Vibration and Acoustics. Manuscript received January 7, 2016; final manuscript received June 23, 2016; published online July 19, 2016. Assoc. Editor: Mahmoud Hussein.

The enhanced capabilities of the CW–CUF approach have already been observed in static and dynamic analyses of aeronautical, civil, and composite structures [28,29]. Numerical assessments have been performed on symmetric and asymmetric three-layered beams with isotropic and orthotropic constraining layers and I-shaped damper. The results have been reported in terms of frequencies and modal loss factors, and they have been compared with 3D numerical solutions and with results available in the literature. The article is organized as follows: Section 1 presents the basic notions of the LE formulation; Section 2 contains the preliminaries for the viscoelastic problem; Section 3 is devoted to the numerical results, and the concluding remarks are given in Sec. 4.

2 The Kinematic Assumption: Lagrange-like Expansions

According to the unified formulation, the displacement field is an expansion of generic cross-sectional functions, F_τ

$$u(x,y,z) = F_\tau(x,z)u_\tau(y) \qquad \tau = 1,2,\ldots,M \tag{1}$$

where u_τ is the vector of the *generalized* displacement, M is the number of terms of the expansion, and in according to the generalized Einstein's notation, τ indicates summation. In this work, the functions, $F_\tau(x, z)$, are Lagrange-like polynomials and the isoparametric formulation is used to deal with arbitrary shape geometries. For the nine-point element (hereafter referred as L9), the interpolation functions are given by

$$\begin{aligned}
F_\tau &= \frac{1}{4}\left(r^2 + rr_\tau\right)\left(s^2 + ss_\tau\right) \qquad \tau = 1,3,5,7\\
F_\tau &= \frac{1}{2}s_\tau^2\left(s^2 - ss_\tau\right)\left(1 - r^2\right) + \frac{1}{2}r_\tau^2\left(r^2 - rr_\tau\right)\left(1 - s^2\right) \qquad \tau = 2,4,6,8\\
F_\tau &= \left(1 - r^2\right)\left(1 - s^2\right) \qquad \tau = 9
\end{aligned} \tag{2}$$

where r and s vary from -1 to $+1$, whereas r_τ and s_τ are the coordinates of the nine points in the natural coordinate frame (see Fig. 1).

The displacement field of a L9 element is therefore

$$\begin{aligned}
u_x &= F_1 u_{x_1} + F_2 u_{x_2} + F_3 u_{x_3} + \cdots + F_9 u_{x_9}\\
u_y &= F_1 u_{y_1} + F_2 u_{y_2} + F_3 u_{y_3} + \cdots + F_9 u_{y_9}\\
u_z &= F_1 u_{z_1} + F_2 u_{z_2} + F_3 u_{z_3} + \cdots + F_9 u_{z_9}
\end{aligned} \tag{3}$$

where $u_{x_1}, \ldots, u_{z_9}$ are the displacement variables of the problem and they represent the translational displacement components of each points of the L9 element. The beam cross section can be discretized by using several L-elements for further refinements. For more details on Lagrange 1D models, the authors suggest to refer to Refs. [30] and [31], where Lagrange elements with 3, 4, 6, and 16 nodes were described.

2.1 Preliminaries and 1D-CUF FEs.

The classical FE technique enables arbitrary shaped cross sections and boundary conditions to be considered. The generalized displacement vector is

$$\mathbf{u}_\tau(y) = N_i(y)\mathbf{q}_{\tau i} \tag{4}$$

where $\mathbf{q}_{\tau i}$ is the nodal displacement vector

$$\mathbf{q}_{\tau i} = \left\{ q_{u_{x_{\tau i}}} \quad q_{u_{y_{\tau i}}} \quad q_{u_{z_{\tau i}}} \right\}^{\mathrm{T}} \tag{5}$$

The Lagrangian shape functions N_i are reported in Ref. [32] (Sec. 5.2.2) for beam elements with two, three, and four nodes. The PVDs is here adopted in order to derive the equations of motion

$$\delta L_{\mathrm{int}} = \delta L_{\mathrm{ext}} + \delta L_{\mathrm{ine}} \tag{6}$$

where δ stands for virtual variation, L_{int} and L_{ine} are the strain and inertial energies, respectively. Assuming that the work of external loadings L_{ext} is null, Eq. (6) becomes

$$\delta L_{\mathrm{ine}} - \delta L_{\mathrm{int}} = \int_V (\delta \mathbf{u}^{\mathrm{T}} \rho \ddot{\mathbf{u}}) dV - \int_V (\delta \boldsymbol{\varepsilon}_p^{\mathrm{T}} \boldsymbol{\sigma}_p + \delta \boldsymbol{\varepsilon}_n^{\mathrm{T}} \boldsymbol{\sigma}_n) dV = 0 \tag{7}$$

where $\ddot{u}$ is the acceleration and, ρ is the material density. The stresses σ and strains ε are grouped as it follows:

$$\begin{aligned}
\boldsymbol{\varepsilon}_p &= \{\varepsilon_{zz} \quad \varepsilon_{xx} \quad \varepsilon_{xz}\}^{\mathrm{T}} \qquad & \boldsymbol{\sigma}_p &= \{\sigma_{zz} \quad \sigma_{xx} \quad \sigma_{xz}\}^{\mathrm{T}}\\
\boldsymbol{\varepsilon}_n &= \{\varepsilon_{zy} \quad \varepsilon_{xy} \quad \varepsilon_{yy}\}^{\mathrm{T}} \qquad & \boldsymbol{\sigma}_n &= \{\sigma_{zy} \quad \sigma_{xy} \quad \sigma_{yy}\}^{\mathrm{T}}
\end{aligned} \tag{8}$$

The subscript p refers to the terms lying on the cross section, while n refers to those lying on the orthogonal planes to the cross section. The linear strain–displacement relations and Hooke's law are, respectively,

$$\begin{aligned}
\boldsymbol{\varepsilon}_p &= \mathbf{D}_p \mathbf{u}\\
\boldsymbol{\varepsilon}_n &= (\mathbf{D}_{ny} + \mathbf{D}_{np})\mathbf{u}
\end{aligned} \tag{9}$$

$$\begin{aligned}
\boldsymbol{\sigma}_p &= \tilde{\mathbf{C}}_{pp}\boldsymbol{\varepsilon}_p + \tilde{\mathbf{C}}_{pn}\boldsymbol{\varepsilon}_n\\
\boldsymbol{\sigma}_n &= \tilde{\mathbf{C}}_{np}\boldsymbol{\varepsilon}_p + \tilde{\mathbf{C}}_{nn}\boldsymbol{\varepsilon}_n
\end{aligned} \tag{10}$$

in which $\mathbf{D}_p$, $\mathbf{D}_{ny}$, and $\mathbf{D}_{np}$ are the linear differential operators reported in Ref. [32].

For isotropic and orthotropic materials, the explicit forms of the coefficients of the $\tilde{\mathbf{C}}$ matrices are reported in Ref. [33]. In this paper, the complex modulus approach has been used to define the viscoelastic materials properties. According to this methodology, the usual engineering moduli are defined as complex quantities. For example, the Young's modulus is

$$E(i\omega) = E_{c0}(\omega) * (1 + i\eta_c(\omega)) \tag{11}$$

where $E_{c0}(\omega)$ is the storage modulus, $\eta_c(\omega)$ is the corresponding material loss factor, and $i = \sqrt{-1}$.

The virtual variation of the strain energy is written in a compact form using Eqs. (1), (4), (9), and (10)

$$\delta L_{\mathrm{int}} = \delta \mathbf{q}_{\tau i}{}^{\mathrm{T}} \mathbf{K}^{ij\tau s} \mathbf{q}_{si} \tag{12}$$

The $\mathbf{K}^{ij\tau s}$ is the complex fundamental nucleus of the stiffness matrix

$$\begin{aligned}
\mathbf{K}^{ij\tau s} = I_l^{ij} \triangleleft & \left(\mathbf{D}_{np}^{\mathrm{T}} F_\tau \mathbf{I}\right)\left[\tilde{\mathbf{C}}_{np}^k \left(\mathbf{D}_p F_s \mathbf{I}\right) + \tilde{\mathbf{C}}_{nn}^k \left(\mathbf{D}_{np} F_s \mathbf{I}\right)\right]\\
& + \left(\mathbf{D}_p^{\mathrm{T}} F_\tau \mathbf{I}\right)\left[\tilde{\mathbf{C}}_{pp}^k \left(\mathbf{D}_p F_s \mathbf{I}\right) + \tilde{\mathbf{C}}_{pn}^k \left(\mathbf{D}_{np} F_s \mathbf{I}\right)\right] \triangleright_\Omega\\
& + I_l^{ij_{,y}} \triangleleft \left[\left(\mathbf{D}_{np}^{\mathrm{T}} F_\tau \mathbf{I}\right)\tilde{\mathbf{C}}_{nn}^k + \left(\mathbf{D}_p^{\mathrm{T}} F_\tau \mathbf{I}\right)\tilde{\mathbf{C}}_{pn}^k\right] F_s \triangleright_\Omega \mathbf{I}_{\Omega y}\\
& + I_l^{i_{,y}j} \mathbf{I}_{\Omega y} \triangleleft F_\tau \left[\tilde{\mathbf{C}}_{np}^k \left(\mathbf{D}_p F_s \mathbf{I}\right) + \tilde{\mathbf{C}}_{nn}^k \left(\mathbf{D}_{np} F_s \mathbf{I}\right)\right] \triangleright_\Omega\\
& + I_l^{i_{,y}j_{,y}} \mathbf{I}_{\Omega y} \triangleleft F_\tau \tilde{\mathbf{C}}_{nn}^k F_s \triangleright_\Omega \mathbf{I}_{\Omega y}
\end{aligned} \tag{13}$$

where

$$\mathbf{I}_{\Omega y} = \begin{bmatrix} 0 & 0 & 1\\ 1 & 0 & 0\\ 0 & 1 & 0 \end{bmatrix} \triangleleft \ldots \triangleright_\Omega = \int_\Omega \ldots d\Omega \tag{14}$$

$$\left(I_l^{ij}, I_l^{ij_{,y}}, I_l^{i_{,y}j}, I_l^{i_{,y}j_{,y}}\right) = \int_l \left(N_i N_j, N_i N_{j_{,y}}, N_{i_{,y}} N_j, N_{i_{,y}} N_{j_{,y}}\right) dy \tag{15}$$

The virtual variation of the inertial energy is

$$\delta L_{\mathrm{ine}} = \int_l \delta \mathbf{q}_{\tau i}^{\mathrm{T}} N_i \left[\int_\Omega \rho^k (F_\tau \mathbf{I})(F_s \mathbf{I})\, d\Omega\right] N_j \ddot{\mathbf{q}}_{sj}\, dy \tag{16}$$

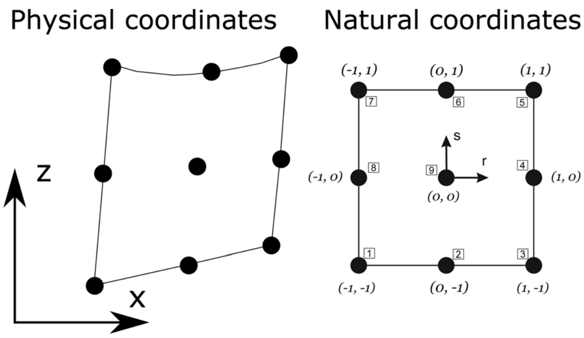

Fig. 1 Coordinates mapping between coordinate systems

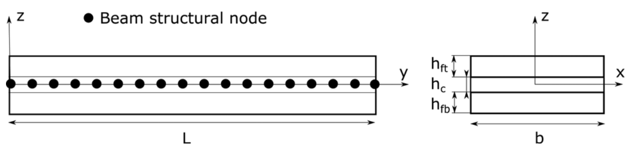

Fig. 2 Dimensions of rectangular cross section beam

where $\ddot{\mathbf{q}}$ is the nodal acceleration vector and ρ^k is the material density of the generic structural components. The last equation can be written in the following compact manner:

$$\delta L_{\text{ine}} = \int_l \boldsymbol{\delta}\mathbf{q}_{\tau i}^{\mathbf{T}} \mathbf{M}^{ij\tau s} \ddot{\mathbf{q}}_{sj}\, dy \tag{17}$$

where $\mathbf{M}^{ij\tau s}$ is the real-valued mass matrix in fundamental nucleus form. Its components are

$$\begin{aligned} &M_{xx}{}^{ij\tau s} = M_{yy}{}^{ij\tau s} = M_{zz}{}^{ij\tau s} = I_l^{ij} \triangleleft (F_\tau \rho^k \mathbf{I} F_s) \triangleright \\ &M_{xy}{}^{ij\tau s} = M_{xz}{}^{ij\tau s} = M_{yx}{}^{ij\tau s} = M_{yz}{}^{ij\tau s} = M_{zx}{}^{ij\tau s} = M_{zy}{}^{ij\tau s} = 0 \end{aligned} \tag{18}$$

Homogeneous equations of motion are solved assuming a periodic solution $\mathbf{q} = \bar{\mathbf{q}}]e^{i\omega^* t}$ in order to determine the complex eigenvalues ($\Lambda_n^* = \Lambda_n + i\,\Lambda_n'$) and corresponding complex eigenvectors ($\bar{\mathbf{q}}_n$) of the system

$$(-\Lambda_n^* \mathbf{M} + \mathbf{K}(\omega_n))\bar{\mathbf{q}}_n = 0 \tag{19}$$

The damped frequencies are related to the real part of complex eigenvalues ($\omega_n = \sqrt{\Lambda_n}$), while the modal loss factors are defined as $\eta_n = (\Lambda_n')/(\Lambda_n)$. Since the storage modulus and the material loss factor may be, in general, functions of the angular vibrational frequency, the eigenvalue problem of Eq. (19) is nonlinear and, hence, it is solved through an iterative process. The convergence of the method is reached when

$$\frac{\| \omega_j - \omega_{j-1} \|}{\omega_{j-1}} \le \varepsilon$$

where ω_j and ω_{j-1} are the current and previous iteration frequencies, respectively, and ε is the tolerance.

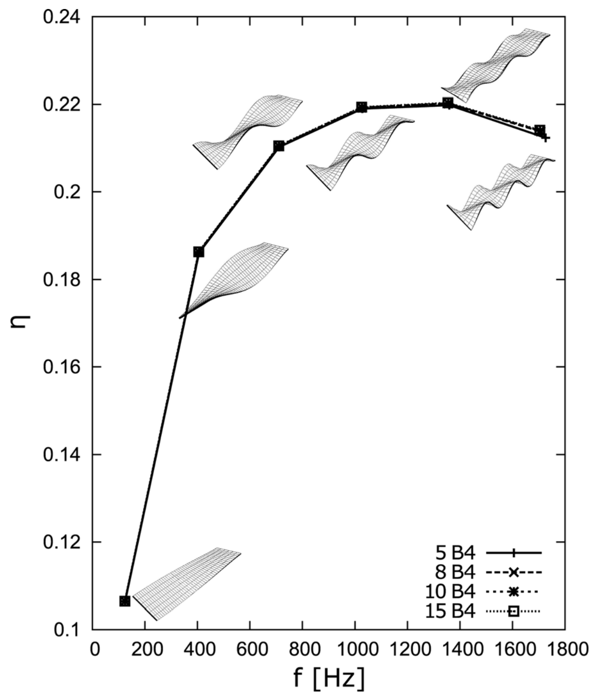

Fig. 3 Root loci related to the first six torsional mode shapes of the asymmetric structure

3 Numerical Results

3.1 Viscoelastic Beams With Isotropic Constraining Layers. A sandwich beam with a rectangular cross section, metallic faces, and a viscoelastic core has been analysed (see Fig. 2). The length and the width of the cantilevered structure have been assumed equal to $L = 0.3\,\text{m}$ and $b = 0.05\,\text{m}$, respectively. The lower and upper constraining faces with thicknesses $h_{fb} = 0.0012$ and $h_{ft} = 0.0008\,\text{m}$, respectively, have been made of aluminum with Young's modulus $E_f = 64\,\text{GPa}$, density $\rho_f = 2695\,\text{kg/m}^{-3}$, and Poisson's ratio $\nu_f = 0.32$. The material properties of the thin

Table 1 Frequencies (Hz) and modal loss factors of the asymmetric beam

	f_1	f_2	f_3	f_4	f_5	f_6	f_7	f_8
Bending frequencies								
Exp. [18]	16	80	210	391	625	908	1241	1622
FEM [18]	16	80	212	395	631	915	1247	1628
5 B4	16.260	83.916	222.92	418.06	670.15	986.91	1373.2	1863.9
8 B4	16.226	83.735	222.36	416.53	665.83	967.02	1320.0	1725.4
10 B4	16.215	83.676	222.20	416.18	665.11	965.38	1316.2	1718.1
15 B4	16.200	83.596	221.98	415.75	664.36	964.07	1313.7	1713.1
Bending loss factors								
Exp. [18]	0.055	0.156	0.206	0.223	0.223	0.216	0.205	0.191
FEM [18]	0.058	0.164	0.214	0.231	0.230	0.220	0.206	0.190
5 B4	0.054	0.165	0.213	0.233	0.234	0.226	0.211	0.193
8 B4	0.054	0.165	0.214	0.234	0.235	0.228	0.216	0.200
10 B4	0.054	0.165	0.214	0.234	0.235	0.228	0.216	0.201
15 B4	0.054	0.165	0.214	0.234	0.235	0.228	0.216	0.201

Table 2 Frequencies, f (Hz), as functions of the core loss factor η_c

η_c		f_1	f_2	f_3	f_4	f_5	f_6	f_7^+	f_8^+
0.1	Ref. [14]	64.075	296.41	743.7	1393.9	2261.09	—	—	—
	Ref. [34]	63.614	294.236	738.028	1382.912	2242.606	3315.226	—	—
	Ref. [10]	64.1	296.6	744.4	1395.6	2264.5	3349.7	—	—
	3D FE[a]	64.524	298.338	749.571	1409.876	2299.435	3425.558	850.224	2567.734
	3D FE[b]	64.417	297.686	747.294	1401.857	2277.416	3373.856	966.230	2921.406
	3D FE[c]	64.374	297.835	747.367	1401.194	2273.752	3363.731	1001.933	3030.627
	LE9	64.373	297.867	747.515	1401.733	2275.652	3369.951	1031.143	3118.251
1.0	Ref. [14]	67.41	302.8	748.6	1396.6	2262.88	—	—	—
	Ref. [34]	67.251	302.307	745.001	1386.887	2245.306	3317.018	—	—
	Ref. [10]	67.4	303.0	749.4	1397.9	2266.3	3350.9	—	—
	3D FE[a]	68.215	306.449	756.402	1413.870	2301.861	3427.000	850.769	2570.417
	3D FE[b]	68.106	305.800	754.256	1405.771	2280.058	3375.561	966.864	2924.931
	3D FE[c]	68.052	305.965	754.345	1405.157	2276.435	3365.485	1002.632	3034.714
	LE9	68.050	306.001	754.503	1405.708	2278.336	3371.720	1031.851	3122.600
1.5	Ref. [14]	69.88	308.85	754.0	1397.7	2265.0	—	—	—
	Ref. [34]	69.816	309.855	753.161	1391.618	2248.594	3319.181	—	—
	Ref. [10]	69.9	309.1	755.2	1401.4	2268.4	3352.3	—	—
	3D FE[a]	70.819	314.047	764.418	1418.096	2304.828	3428.824	851.185	2572.127
	3D FE[b]	70.707	313.400	762.404	1410.439	2283.277	3377.640	967.333	2926.937
	3D FE[c]	70.645	313.575	762.520	1409.877	2279.704	3367.621	1003.142	3036.941
	LE9	70.643	313.614	762.687	1410.441	2281.621	3373.871	1032.369	3124.899

Note: "+": frequencies related to torsional mode shapes.

core ($h_c = 0.0001016\,\text{m}$) have been assumed frequency-dependent, according to the following viscoelastic laws:

$$G_c = 2.783 - \frac{1.023}{z_G} \qquad z_G = 0.394 + 0.0003736f$$
$$\eta_c = 1.683 + \frac{0.001468}{z_\eta} - \frac{0.5274}{z_\eta^{0.25}} \qquad z_\eta = 0.005 + 0.0006134f$$

where f (Hz) is the natural frequency. A convergence study has been performed to evaluate the effects of the number of four-node beam elements (B4) along the longitudinal axis. For each mathematical model, three LE9 (one per each layer) have been used to discretize the cross section. The results related to the first eight flexural mode shapes are listed in Table 1 where, for comparison purposes, numerical and experimental results presented in Ref. [18] are reported. The comparisons have revealed that the proposed approach yields values close to the reference solutions and, eight B4 elements ensure the convergence of frequencies and modal loss factors for the considered mode shapes. Figure 3 shows the root loci for the first six torsional mode shapes obtained from the above mathematical models. The curves related to the different discretizations are almost overlapped since the number of beam elements does not significantly affect torsional eigenvalues. Furthermore, it is noteworthy that the torsional loss factors have the same order of magnitude of those related to the flexural modes of Table 1.

In the second assessment, a symmetric sandwich beam has been considered. The structure consisted of a viscoelastic core with thickness $h_c = 0.127\,\text{mm}$ constrained between two metallic layers with Young's modulus $E_f = 69\,\text{GPa}$, density $\rho_f = 2766\,\text{kg/m}^{-3}$,

Table 3 Loss factors, η (%), as functions of the core loss factor η_c

η_c		f_1	f_2	f_3	f_4	f_5	f_6	f_7^+	f_8^+
0.1	Ref. [14]	2.815	2.424	1.54	0.889	0.573	—	—	—
	Ref. [34]	2.813	2.426	1.544	0.891	0.574	0.392	—	—
	Ref. [10]	2.81	2.42	1.54	0.88	0.57	0.39	—	—
	3D FE[a]	2.815	2.410	1.515	0.857	0.537	0.354	0.149	0.161
	3D FE[b]	2.816	2.417	1.530	0.877	0.561	0.378	0.151	0.169
	3D FE[c]	2.810	2.415	1.532	0.881	0.566	0.384	0.157	0.178
	LE9	2.809	2.415	1.532	0.881	0.566	0.384	0.152	0.176
1.0	Ref. [14]	20.22	21.77	15.02	8.81	5.7	—	—	—
	Ref. [34]	20.202	21.786	15.056	8.833	5.719	3.909	—	—
	Ref. [10]	20.2	21.7	15.0	8.8	5.7	3.8	—	—
	3D FE[a]	20.027	21.411	14.704	8.480	5.350	3.527	1.418	1.470
	3D FE[b]	20.031	21.477	14.839	8.678	5.578	3.772	1.431	1.496
	3D FE[c]	19.984	21.443	14.853	8.714	5.628	3.828	1.480	1.558
	LE9	19.781	21.201	14.776	8.703	5.629	3.829	1.429	1.517
1.5	Ref. [14]	22.956	29.625	21.9	13.095	8.52	—	—	—
	Ref. [34]	22.938	29.650	21.935	13.128	8.541	5.845	—	—
	Ref. [10]	22.95	29.55	21.75	13.05	8.4	5.7	—	—
	3D FE[a]	22.679	28.956	21.317	12.584	7.986	5.279	2.059	2.086
	3D FE[b]	22.678	28.965	21.494	12.872	8.323	5.644	2.076	2.109
	3D FE[c]	22.626	28.908	21.514	12.923	8.398	5.727	2.146	2.185
	LE9	22.333	28.319	21.272	12.877	8.390	5.726	2.068	2.119

Note: "+": frequencies related to torsional mode shapes.

Table 4 Maxwell series terms at 27 °C and 20 °C of 3M ISD112

	27 °C			20 °C		
j	G_0 (MPa)	Δ_j	Ω_j (rad s^{-1})	G_0 (MPa)	Δ_j	Ω_j (rad s^{-1})
1	0.5	0.746	468.7	0.0511	2.8164	31.1176
2	—	3.265	4742.4	—	13.1162	446.4542
3	—	43.284	71532.5	—	45.4655	5502.5318

Poisson's ratio $\nu_f = 0.3$, and thickness $h_{fb} = h_{ft} = 1.524$ mm. The beam length and the width dimension have been assumed equal to $L = 177.8$ mm and $b = 12.7$ mm, respectively. This beam configuration was extensively analysed in previous works by assuming either constant or frequency-dependent properties of the core. For the case of constant values of η_c, the storage core modulus, the density, and the Poisson's ratio of the core have been assumed equal to $E_{c0} = 1.794$ MPa, $\rho_c = 968.13$ kg/m^{-3}, and $\nu_c = 0.3$, respectively. Tables 2 and 3 list the damped frequencies and the modal loss factors for different η_c. The values obtained with three LE9 are compared with solutions available in the literature and those derived from three different 3D FE models. In particular, the 3D FE^a model consisted of two eight-node brick elements along the width direction, three elements (one per each layer) along the thickness and 25 elements along the longitudinal axis (1575 degrees-of-freedom (DOF)). The second solution (3D FE^b) has been obtained by using a twice number of elements through the three directions (9450DOFs). Finally, the 3D FE^c mesh (63,000DOFs) has been built by using 9, 20, and 100 elements along the thickness, the width, and the length of the beam, respectively. For the flexural mode shapes, the comparisons have revealed a significant agreement between the various approaches, both in terms of frequencies and modal loss factors. As far as torsional deformations (seventh and eighth columns) are concerned, the first two solid solutions have predicted lower torsional frequencies respecting to the CUF and 3D FE^c results. The first two models, which are clearly not convergent, were built using FEs with large values of dimensional ratios (A.R. $\simeq$ 150). The significant dimensional distortion has led to an inaccurate prediction of torsional frequencies with respect to the finest solid solution and, the appearance of spurious mode shapes. It should be noted that the proposed beam solution has required the same number of DOFs of the coarsest solid model (1575DOFs). For the frequency-dependent case [10], the core has been considered made of 3M ISD112 viscoelastic material whose mechanical properties vary according to the following equation:

$$G_c(\omega) = G_0 \left(1 + \sum_{j=1}^{3} \frac{\Delta_j \, \omega}{\omega - i\,\Omega_j} \right) \tag{20}$$

where G_0 is the shear modulus of the delayed elasticity and (Δ_j, Ω_j) the Maxwell parameters obtained by master curves fitting (see Table 4). The density of the 3M ISD112 material and its Poisson's ratio have been assumed equal to $\rho_c = 1600$ kg/m^{-3} and $\nu_c = 0.49$, respectively. The frequencies and loss factors related to the first four bending modes are shown in Table 5. For comparison purposes, the results obtained from the *approached complex eigenmodes* (ACMs) and *exact complex eigenmodes* (ECMs) techniques presented in Ref. [10] have been reported. The analyses have been performed adopting either 9- or 16-node Lagrange elements (one element per each layer). For both temperature values, the comparisons have pointed out the significant agreement with the reference solutions. For the first torsional mode, as expected, the LE16 model predicts lower frequencies and higher loss factors than those obtained from the LE9 discretization.

3.2 Viscoelastic Beams With Orthotropic Constraining Layers. In order to evaluate the effects of lamination sequence on the dynamics of viscoelastic structures, the constraining layers have been considered made of orthotropic material with $E_{11} = 138.6$ MPa, $E_{22} = E_{33} = 8.27$ MPa, $\nu_{12} = \nu_{13} = \nu_{23} = 0.3$, $G_{12} = G_{13} = G_{23} = 4.12$ MPa and, $\rho_f = 1824$ kg/m^{-3}. The density and Poisson's ratio of the core have been assumed equal to $\rho_c = 999$ kg/m^{-3} and $\nu_c = 0.3$, respectively, while the Young's modulus has been again assumed constant ($E_{c0} = 1.794$ MPa). First, assuming $\eta_c = 0.6$ and the fiber angle as a problem parameter according to the [θ/core/$-\theta$] scheme, the analyses have been performed with three LE16 and three LE9 models. Table 6 lists frequencies and the modal loss factors related to the first four flexural mode shapes. The comparisons with 3D FE^c solutions (63,000DOFs) have demonstrated the significant accuracy of the CW approach. As expected, the use of the higher-order displacement expansion (LE16) slightly improves the results. Moreover, Fig. 4 shows the variations of frequencies and modal loss factors as functions of the fiber angle for the first torsional mode. As shown in Fig. 4(*a*), the use of cubic expansions within Lagrange elements determines significant improvements in the computation of frequencies. Conversely, the CUF curves related to the modal loss factors (see Fig. 4(*b*)) are almost overlapped.

Second, the symmetric lamination sequence [θ/core/θ] has been evaluated. This configuration involves significant bending-torsion coupling. The results derived from analyses performed with the 16-node Lagrange elements are graphically shown in Fig. 5 for $\eta_c = 1.5$. In particular, Figs. 5(*a*) and 5(*b*) show frequencies and loss factors related to modes dominated by the bending whereas the remaining graphs, Figs. 5(*c*) and 5(*d*), concern the first torsional mode shape. As usual, 3D solutions have been taken as reference values. The comparisons have pointed out the good agreement between the two approaches also for the symmetric lamination sequence.

3.3 The I-Beam Damper. The I-beam acts as a constraining layer by inducing thickness deformation in the adhesive and providing the required bending stiffness. The considered structure and the section dimensions are shown in Fig. 6(*a*). Both base and

Table 5 Frequencies (Hz) and modal loss factors for the viscoelastic law of Eq. (20)

	f_1	f_2	f_3	f_4	f_5^+	η_1	η_2	η_3	η_4	η_5^+
27 °C										
ACM [10]	65.04	322.47	839.97	1556.38	—	0.159	0.260	0.288	0.270	—
ECM [10]	65.34	326.08	849.49	1567.53	—	0.156	0.255	0.278	0.269	—
LE16	65.801	330.750	865.909	1595.476	1025.140	0.158	0.261	0.284	0.272	0.0474
LE9	65.809	330.811	866.110	1595.992	1042.472	0.158	0.261	0.284	0.272	0.0469
20 °C										
ACM [10]	61.96	314.58	821.85	1530.85	—	0.262	0.198	0.169	0.0963	—
ECM [10]	63.07	316.54	823.29	1530.60	—	0.196	0.187	0.160	0.0948	—
LE16	64.992	323.168	840.875	1546.769	1024.844	0.220	0.199	0.156	0.0864	0.0210
LE9	65.001	323.228	841.071	1547.264	1042.197	0.220	0.199	0.156	0.0863	0.0205

Note: "+": frequencies and loss factors related to torsional mode shape.

Table 6 Frequencies (Hz) and modal loss factors for the viscoelastic beam with orthotropic constraining layers ($\eta_c = 0.6$)

θ deg		0	15	30	45	60	75	90
3D	f_1	102.263	82.444	55.721	40.213	34.779	33.162	33.040
	f_2	478.762	417.611	293.802	211.338	182.641	172.425	171.834
	f_3	1227.24	1074.70	743.966	517.812	441.515	418.035	416.614
	f_4	2324.74	2017.15	1373.62	923.191	770.612	731.512	728.888
LE16	f_1	102.268	82.697	56.015	40.394	34.862	33.524	33.391
	f_2	478.768	419.382	295.801	212.536	183.162	176.298	175.643
	f_3	1226.93	1079.92	750.022	521.135	442.815	425.718	424.154
	f_4	2323.15	2027.71	1386.80	930.128	773.027	740.492	737.627
LE9	f_1	102.280	83.571	56.807	40.656	34.901	33.526	33.391
	f_2	479.047	426.079	301.979	214.841	183.527	176.319	175.649
	f_3	1228.68	1100.90	771.971	530.518	444.259	425.795	424.180
	f_4	2329.33	2072.59	1440.67	956.961	777.246	740.704	737.706
3D	η_1	0.174	0.087	0.051	0.046	0.044	0.043	0.043
	η_2	0.105	0.096	0.115	0.140	0.148	0.149	0.148
	η_3	0.054	0.070	0.110	0.156	0.176	0.179	0.179
	η_4	0.028	0.052	0.095	0.141	0.169	0.174	0.175
LE16	η_1	0.173	0.086	0.050	0.045	0.043	0.042	0.042
	η_2	0.105	0.095	0.113	0.139	0.148	0.148	0.148
	η_3	0.054	0.069	0.108	0.154	0.175	0.178	0.178
	η_4	0.028	0.051	0.093	0.139	0.167	0.173	0.173
LE9	η_1	0.173	0.084	0.049	0.044	0.043	0.042	0.042
	η_2	0.105	0.092	0.110	0.136	0.147	0.148	0.148
	η_3	0.054	0.068	0.105	0.150	0.174	0.178	0.178
	η_4	0.028	0.051	0.091	0.134	0.166	0.173	0.173

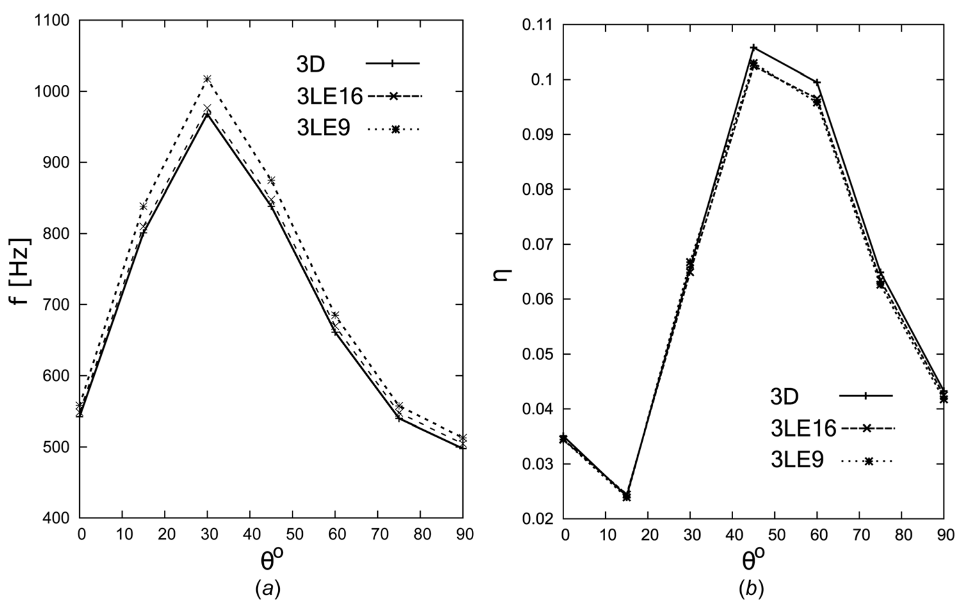

Fig. 4 Frequencies (*a*) and modal loss factors and (*b*) related to the first torsional mode shape of the orthotropic beam [θ/core/$-\theta$]. $\eta_c = 0.6$

I-beam are made of aluminum with Young's modulus $E_f = 69$ GPa, density $\rho_f = 2766$ kg/m^{-3} and, $\nu_f = 0.3$. The mechanical properties of the adhesive are the same of those used in Sec. 2, assuming η_c equal to 1.5. The analyses have been performed by using the 1D-CUF LE9 elements as shown in Fig. 6(*a*). The results are shown in Fig. 7, where the first ten modes, frequencies and modal loss factors are compared with those obtained from a convergent 3D FE solution (see Fig. 6(*b*)). Besides the bending modes, the proposed 1D element enables the structure kinematics to be described by detecting torsional, shear, and shell-type deformations. Despite the structure being stubby, the agreement of 1D-CUF results with the reference solution is significant, especially in terms of frequencies. As expected, the modal shapes characterized by the highest damping values mainly involve the motions of the base since the viscoelastic adhesive undergoes to significant deformations (see Figs. 7(*e*), 7(*g*), and 7(*h*)).

4 Conclusions

New beam FEs based on the CW approach have been used for the study of the dynamics of structures with passive damping. The higher-order beam elements have been obtained through the CUF.

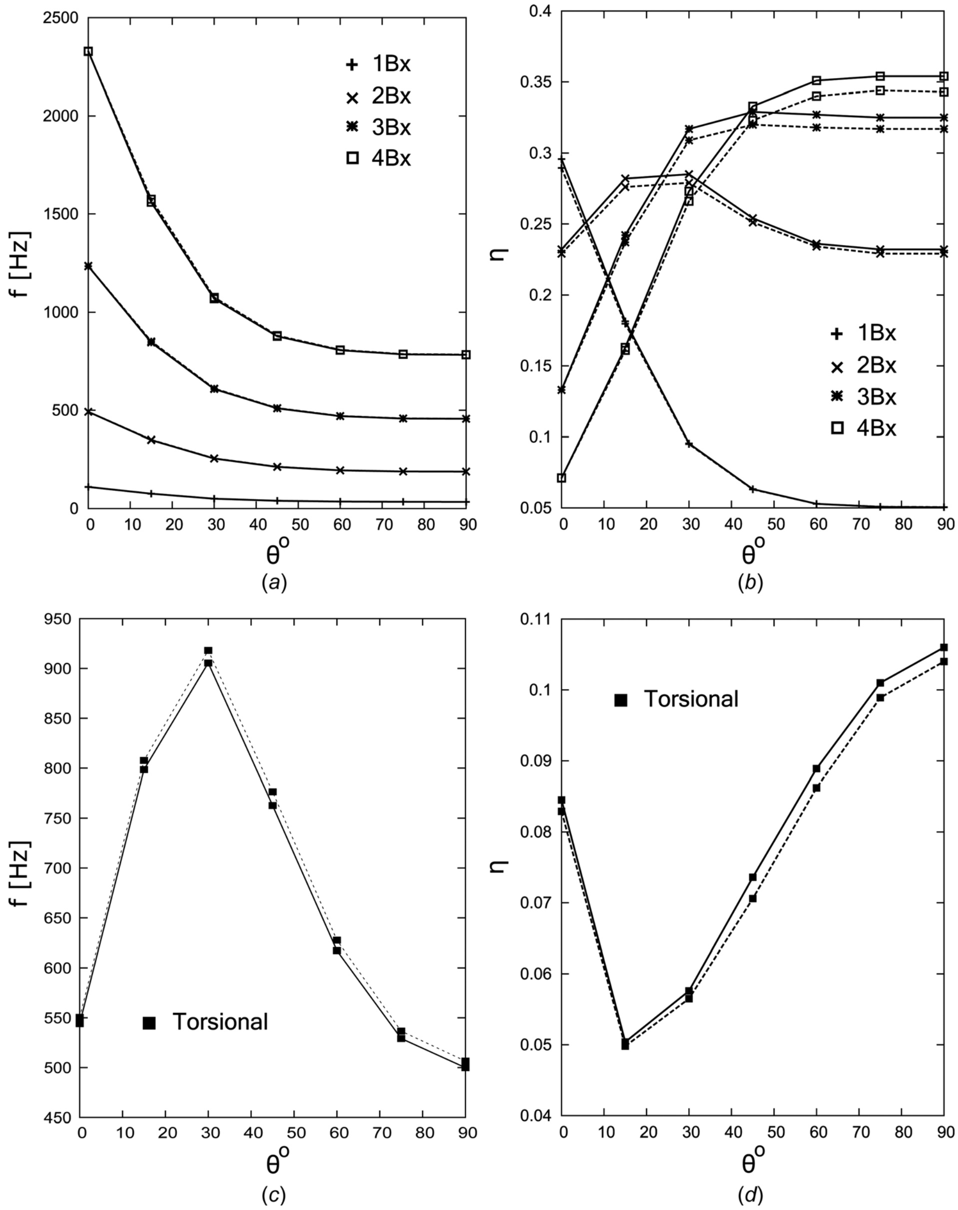

Fig. 5 Frequencies and modal loss factors related to the first mode shapes of the orthotropic beam [θ/core/θ]. $\eta_c = 1.5$. "—": 3D FE, "– – –": 3L16 (*a*) bending frequencies, (*b*) bending loss factors, (*c*) torsional frequencies, and (*d*) torsional loss factors.

The complex modulus approach was adopted in order to describe the damping characteristics of viscoelastic materials. The material properties were considered either constant or frequency-dependent. Numerical simulations were performed on beamlike structures with rectangular and I-shaped section. The constraining layers were considered made of both metallic and orthotropic materials. The comparisons with results available in the literature and 3D FE solutions pointed out the valuable capabilities of the

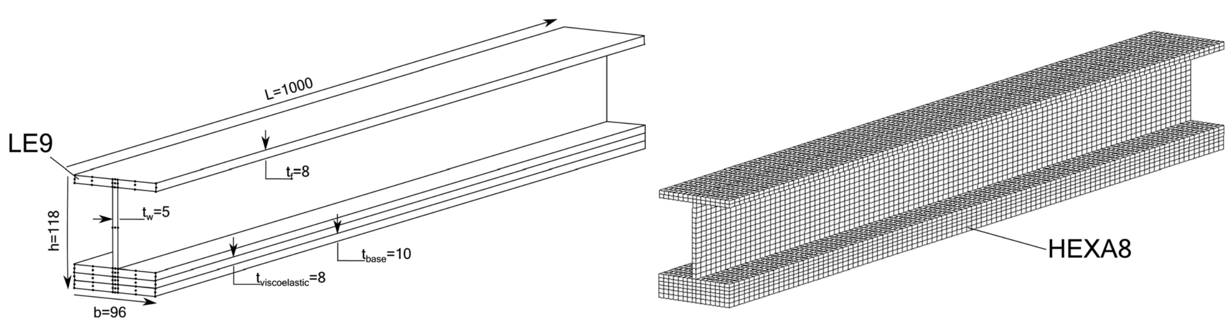

Fig. 6 Dimensions (mm) and numerical models for the I-beam damper: (*a*) LE9 model (5475DOFs) and (*b*) solid model (56,400DOFs)

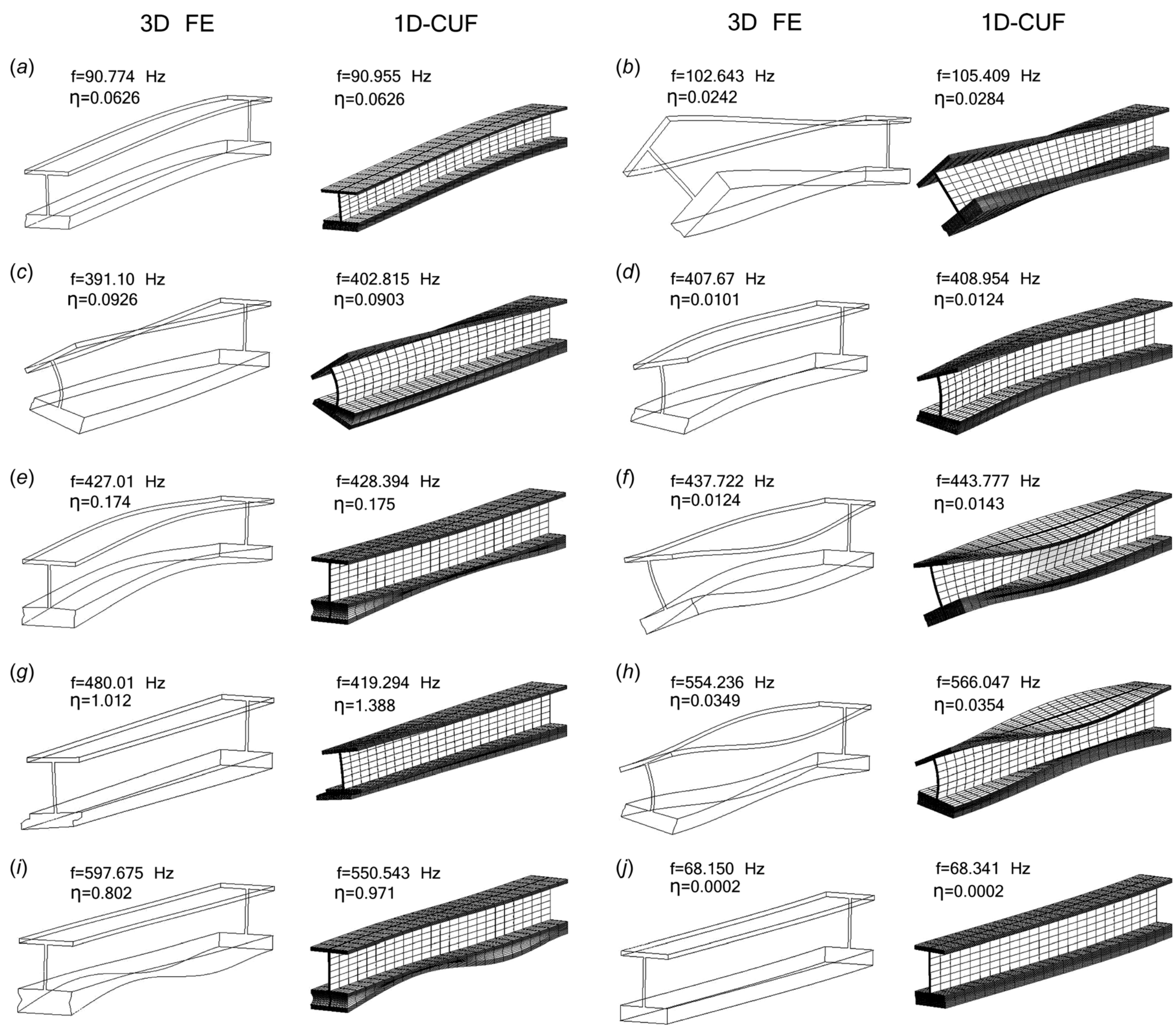

Fig. 7 Mode shapes, frequencies, and modal loss factors of the cantilevered I-beam damper: $\eta_c = 1.5$ (*a*) $f = 90.774$ Hz, $\eta = 0.0626$, $f = 90.955$ Hz, $\eta = 0.0626$, (*b*) $f = 102.643$ Hz, $\eta = 0.0242$, $f = 105.409$ Hz, $\eta = 0.0284$, (*c*) $f = 391.10$ Hz, $\eta = 0.0926$, $f = 402.815$ Hz, $\eta = 0.0903$, (*d*) $f = 407.67$ Hz, $\eta = 0.0101$, $f = 408.954$ Hz, $\eta = 0.0124$, (*e*) $f = 427.01$ Hz, $\eta = 0.174$, $f = 428.394$ Hz, $\eta = 0.175$, (*f*) $f = 437.722$ Hz, $\eta = 0.0124$, $f = 443.777$ Hz, $\eta = 0.0143$, (*g*) $f = 480.01$ Hz, $\eta = 1.012$, $f = 419.294$ Hz, $\eta = 1.388$, (*h*) $f = 554.236$ Hz, $\eta = 0.0349$, $f = 566.047$ Hz, $\eta = 0.0354$, (*i*) $f = 597.675$ Hz, $\eta = 0.802$, $f = 550.543$ Hz, $\eta = 0.971$, and (*j*) $f = 68.150$ Hz, $\eta = 0.0002$, $f = 68.341$ Hz, $\eta = 0.0002$

proposed method in the study of damped structures. Besides the bending frequencies, which are typically provided by the beam approach, the 1D-CUF elements have enabled the torsional, shell-like, and coupled modes to be investigated. This capability may be extremely useful when viscoelastic materials are used to passively control dynamic instabilities, for example, the bending-torsional flutter and, instabilities of rotating structures.

References

[1] Zheng, L., Qiu, Q., Wan, H., and Zhang, D., 2014, "Damping Analysis of Multilayer Passive Constrained Layer Damping on Cylindrical Shell Using Transfer Function Method," ASME J. Vib. Acoust., **136**(3), p. 031001.

[2] Rao, M. D., 2003, "Recent Applications of Viscoelastic Damping for Noise Control in Automobiles and Commercial Airplanes," J. Sound Vib., **262**(3), pp. 457–474.

[3] Rouleau, L., Deü, J.-F., Legay, A., Sigrist, J.-F., Le Lay, F., and Marin-Curtoud, P., 2012, "A Component Mode Synthesis Approach for Dynamic Analysis of Viscoelastically Damped Structures," 10th World Congress on Computational Mechanics (WCCM 2012), Sao Paulo, Brazil, July 8–13, Vol. 229, p. 231.

[4] Roylance, D., 2001, "Engineering Viscoelasticity," Department of Materials Science and Engineering, Massachusetts Institute of Technology, Cambridge MA, Vol. 2139, pp. 1–37.

[5] Slater, J. C., Belvin, W. K., and Inman, D. J., 1993, "A Survey of Modern Methods for Modeling Frequency Dependent Damping in Finite Element Models," Proc. SPIE **1923**, pp. 1508–1512.

[6] Zhang, S. H., and Chen, H. L., 2006, "A Study on the Damping Characteristics of Laminated Composites With Integral Viscoelastic Layers," Compos. Struct., **74**(1), pp. 63–69.

[7] Moita, J., Araújo, A., Soares, C. M., and Soares, C. M., 2013, "Finite Element Model for Damping Optimization of Viscoelastic Sandwich Structures," Adv. Eng. Software, **66**, pp. 34–39.

[8] Ferreira, A., Araújo, A., Neves, A., Rodrigues, J., Carrera, E., Cinefra, M., and Soares, C. M., 2013, "A Finite Element Model Using a Unified Formulation for the Analysis of Viscoelastic Sandwich Laminates," Composites, Part B, **45**(1), pp. 1258–1264.

[9] Abdoun, F., Azrar, L., Daya, E., and Potier-Ferry, M., 2009, "Forced Harmonic Response of Viscoelastic Structures by an Asymptotic Numerical Method," Comput. Struct., **87**(1), pp. 91–100.

[10] Bilasse, M., Daya, E., and Azrar, L., 2010, "Linear and Nonlinear Vibrations Analysis of Viscoelastic Sandwich Beams," J. Sound Vib., **329**(23), pp. 4950–4969.

[11] Boudaoud, H., Belouettar, S., Daya, E. M., and Potier-Ferry, M., 2009, "A Numerical Method for Nonlinear Complex Modes With Application to Active–Passive Damped Sandwich Structures," Eng. Struct., **31**(2), pp. 284–291.

[12] Kerwin, E. M., Jr., 1959, "Damping of Flexural Waves by a Constrained Viscoelastic Layer," J. Acoust. Soc. Am., **31**(7), pp. 952–962.

[13] Di Taranto, R., 1965, "Theory of Vibratory Bending for Elastic and Viscoelastic Layered Finite-Length Beams," ASME J. Appl. Mech., **32**(4), pp. 881–886.

[14] Mead, D., and Markus, S., 1969, "The Forced Vibration of a Three-Layer Damped Sandwich Beam With Arbitrary Boundary Conditions," J. Sound Vib., **10**(2), pp. 163–175.

[15] Yan, M.-J., and Dowell, E., 1972, "Governing Equations for Vibrating Constrained-Layer Damping Sandwich Plates and Beams," ASME J. Appl. Mech., **39**(4), pp. 1041–1046.

[16] Rao, D., 1978, "Frequency and Loss Factors of Sandwich Beams Under Various Boundary Conditions," J. Mech. Eng. Sci., **20**(5), pp. 271–282.
[17] Bhimaraddi, A., 1995, "Sandwich Beam Theory and the Analysis of Constrained Layer Damping," J. Sound Vib., **179**(4), pp. 591–602.
[18] Barkanov, E., Skukis, E., and Petitjean, B., 2009, "Characterisation of Viscoelastic Layers in Sandwich Panels Via an Inverse Technique," J. Sound Vib., **327**(3), pp. 402–412.
[19] Rikards, R., Chate, A., and Barkanov, E., 1993, "Finite Element Analysis of Damping the Vibrations of Laminated Composites," Comput. Struct., **47**(6), pp. 1005–1015.
[20] Koutsawa, Y., Charpentier, I., Daya, E. M., and Cherkaoui, M., 2008, "A Generic Approach for the Solution of Nonlinear Residual Equations—Part I: The Diamant Toolbox," Comput. Methods Appl. Mech. Eng., **198**(3), pp. 572–577.
[21] Berthelot, J.-M., Assarar, M., Sefrani, Y., and El Mahi, A., 2008, "Damping Analysis of Composite Materials and Structures," Compos. Struct., **85**(3), pp. 189–204.
[22] Vallala, V., Ruimi, A., and Reddy, J., 2012, "Nonlinear Viscoelastic Analysis of Orthotropic Beams Using a General Third-Order Theory," Compos. Struct., **94**(12), pp. 3759–3768.
[23] Suzuki, K., Kageyama, K., Kimpara, I., Hotta, S., Ozawa, T., Kabashima, S., and Ozaki, T., 2003, "Vibration and Damping Prediction of Laminates With Constrained Viscoelastic Layers–Numerical Analysis by a Multilayer Higher-Order-Deformable Finite Element and Experimental Observations," Mech. Adv. Mater. Struct., **10**(1), pp. 43–75.
[24] Kosmatka, J., and Liguore, S., 1993, "Review of Methods for Analyzing Constrained-Layer Damped Structures," J. Aerosp. Eng., **6**(3), pp. 268–283.
[25] Moreira, R., and Rodrigues, J. D., 2004, "Constrained Damping Layer Treatments: Finite Element Modeling," J. Vib. Control, **10**(4), pp. 575–595.
[26] Vasques, C., and Rodrigues, J. D., 2011, *Vibration and Structural Acoustics Analysis: Current Research and Related Technologies*, Springer Science & Business Media, The Netherlands.
[27] Carrera, E., Cinefra, M., Petrolo, M., and Zappino, E., 2014, *Finite Element Analysis of Structures Through Unified Formulation*, Wiley, Chichester, UK.
[28] Carrera, E., Filippi, M., Mahato, P. K., and Pagani, A., 2014, "Advanced Models for Free Vibration Analysis of Laminated Beams With Compact and Thin-Walled Open/Closed Sections," J. Compos. Mater., **49**(7), pp. 2085–2101.
[29] Carrera, E., Filippi, M., Mahato, P., and Pagani, A., 2016, "Accurate Static Response of Single-and Multi-Cell Laminated Box Beams," Compos. Struct., **136**, pp. 372–383.
[30] Carrera, E., and Petrolo, M., 2012, "Refined Beam Elements With Only Displacement Variables and Plate/Shell Capabilities," Meccanica, **47**(3), pp. 537–556.
[31] Carrera, E., and Petrolo, M., 2012, "Refined One-Dimensional Formulations for Laminated Structure Analysis," AIAA J., **50**(1), pp. 176–189.
[32] Carrera, E., Giunta, G., and Petrolo, M., 2011, *Beam Structures: Classical and Advanced Theories*, Wiley, Chichester, UK.
[33] Carrera, E., and Filippi, M., 2014, "Variable Kinematic One-Dimensional Finite Elements for the Analysis of Rotors Made of Composite Materials," ASME J. Eng. Gas Turbines Power, **136**(9), p. 092501.
[34] Arikoglu, A., and Ozkol, I., 2010, "Vibration Analysis of Composite Sandwich Beams With Viscoelastic Core by Using Differential Transform Method," Compos. Struct., **92**(12), pp. 3031–3039.